An aerostatic pad with an internal pressure control

An aerostatic pad with an internal pressure control

Luigi Lentini [1,*], *Federico* Colombo [1] , *Terenziano* Raparelli [1], *Andrea* Trivella [1], *Vladimir* Viktorov [1]

[1]Politecnico di Torino, Corso Duca degli Abruzzi 24, 10129, Torino, Italy.

Abstract. Because of their almost zero friction and wear, aerostatic pads are widely used in applications where very precise positioning is required. However, this kind of bearing suffers from poor damping and low specific stiffness. This paper presents a new compensation strategy to increase air pad stiffness. This method exploits a custom-built pneumatic valve which can be easily integrated with any commercial pad. The design and the working principle of the proposed system are described and studied with the aid of a lumped parameter model. The effectiveness of the proposed compensation is numerically and experimentally evaluated. The results demonstrate that the solution represents a good and cost-effective method to enhance the static stiffness of aerostatic pads.

1 Introduction

The almost zero friction and wear of aerostatic bearings make it possible to obtain very smooth and precise motions. To this regard, air pads are widely used in high precision applications, e.g., metrology, measuring and tool machines [1].

However, aerostatic pads suffer from poor damping and relatively low stiffness. Various methods can be employed to increase air pad performance. As regards stationary conditions, the most sought outcomes are increasing load capacity and stiffness and reducing air consumption. Meanwhile, concerning dynamic performance, increased bandwidth and damping are expected. One of the first solutions proposed was machining shallow grooves on the active surface of bearings (compound restrictors) [2–5]. However, experimental and numerical investigations [5, 6] demonstrate that the presence of the additional volumes of these grooves can significantly reduce bearing damping, even leading to instability.

The use of active and passive compensation methods [7] represents an alternative and valuable solution to increase air bearing stiffness reducing the occurrence of instability. Passive compensation methods use components whose functioning requires only the energy associated with the supply pressure of the bearing, e.g., pneumatic valves and compliant elements. Conversely, actively compensated bearings are equipped with elements that require external sources of energy for their functioning, e.g., sensors, controllers and actuators.

* Corresponding author: luigi.lentini@polito.it

The use of movable or elastic orifices are among the more adopted passive compensation strategies. Yoshimoto et al. [8] designed an aerostatic thrust bearing with a self-controlled restrictor. It consists in the integration of a floating disk inside the supply system of the bearing. This solution exploits the pressure acting on the two sides of the floating disk to control the air flow supplying the air gap. Results demonstrate that by using this method bearings may exhibit a level of static stiffness ten times higher than conventional aerostatic thrust bearings. Similar results were obtained by Newgard et al. [9] who proposed the use of elastic orifices to improve air pad performance. It was found that air bearing stiffness can be significantly enhanced if the compliance of these restrictors is suitably selected, depending on the applied load. Ghodsiyeh et al. [10, 11] experienced the use of a custom-built diaphragm valve to increase air pad stiffness. In the presence of load variations, the valve makes it possible to increase the stiffness by a suitable regulation of the air supplied to the pad. Chen and Lin [12] proposed a disk-spring compensator to increase the static and dynamic performance bearing.

Despite their relatively low costs and simple design, passive compensation solutions prove less effective than their active counterpart. Because of the presence of sensors, actuators and controllers, actively compensated bearings may exhibit infinite static stiffness and higher bandwidth. In view of their high dynamic performance, piezoelectric actuators are used in the majority of the existent active compensation systems. Al Bender [13] and Aguirre et al. [14] integrated three piezoelectric actuators in their active pad with variable concavity. Colombo et al. [15, 16] used the same type of actuator to obtain air pads with an active geometrical compensation. In this solution, the stroke of the actuator makes it possible to compensate for air gap variations by modifying the bearing thickness. As well as deforming compliant structures, piezo electric actuators were also employed to regulate the gas supplied to the clearance, as proposed by Morosi and Santos [17, 18] and Pierart and Santos [19].

Despite their remarkable effectiveness, the application of active compensation solutions is hampered by their higher complexity and costs.

This paper presents a new low-cost active compensation solution for aerostatic pads. A pneumatic valve, actuated through an internal pressure control, is used to modify the static behavior of a commercial pad. The functioning and the effectiveness of the method are presented along with the valve design. The performance of the system is assessed through experimental and numerical analysis. The numerical results are obtained with the aid of a lumped parameter model that was developed using the pseudo-unsteady method [20].

2 The compensated pad

Figure 1 shows a photograph of the proposed active pad. It consists in the integration of a conventional commercial air pad with a custom-built pneumatic valve. The aerostatic pad has a rectangular base of 110x50 mm^2 and presents four supply holes with a diameter of 0.5 mm which are located in the middle of a grooved rectangular supply line of dimensions 80x30 mm^2. These grooves have a triangular cross-section of depth h_g=60 μm and base w_g=0.3 mm (see Figure 2). Moreover, the active surface of the pad presents a back-pressure hole used for to evaluate the air gap pressure. The working principle of the system was inspired by different previous solutions. The first one is an active solution to control the position of an aerostatic journal-bearing [21,22] meanwhile the second one was a passive compensation solution to improve the static performance of aerostatic pads [10,11] . Figure 3 shows a cross-section of the valve. The valve presents four chambers (1, 2, 3, 4), a nozzle (5) ($d_n = 1\ mm$), three rubber diaphragms (6) and a shutter (7). The external chambers (1, 2) are supplied with a constant feeding pressure of 0.5 absolute MPa, whereas chambers 3 and 4 are supplied with a feedback pressure (3) and a constant reference pressure (4), respectively. The rubber

diaphragms are clamped to the shutter and are necessary to seal the chambers. The stiffness of the membranes k_m was selected to provide a suitable stroke to the shutter. The inflow that the valve supplies to the pad is strictly related to the distance between the nozzle and the shutter (x).

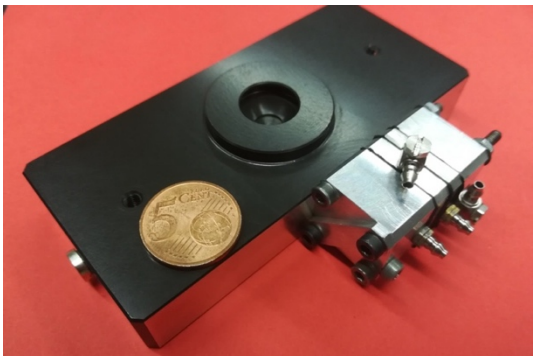

Fig. 1: A photograph of the actively compensated with internal pressure control.

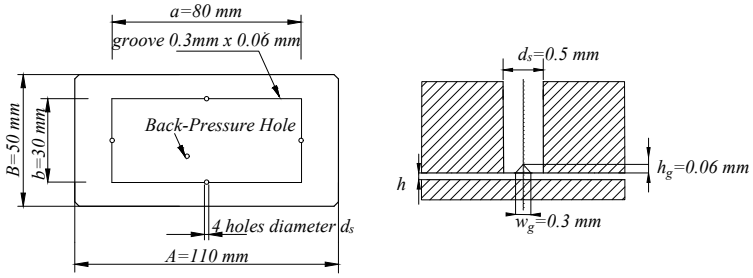

Fig. 2: Geometry of the commercial pad.

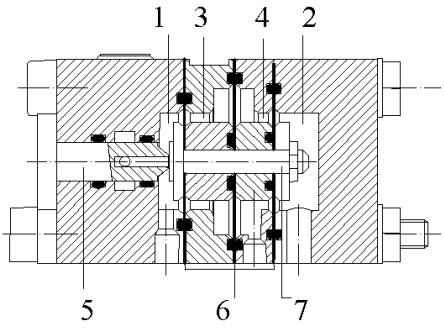

Fig. 3: Cross-section of the pneumatic valve.

This distance is defined on the basis of the force acting on the shutter. Once the supply pressure P_{supply} within chambers 1 and 2 has been defined, the performance of the air pad

changes as the reference pressure P_{Ref} in chamber 4 and the initial nozzle-shutter distance x are modified. This increase of pressure produces a downward displacement of the shutter and an increase of the distance x. In turn, the increase of x induces a rise in the air flow supplied to the pad, which tends to restore the initial air gap height. Conversely, the opposite holds in the presence of load reductions. Figure 4 shows a scheme useful in order to clarify the functioning of the system.

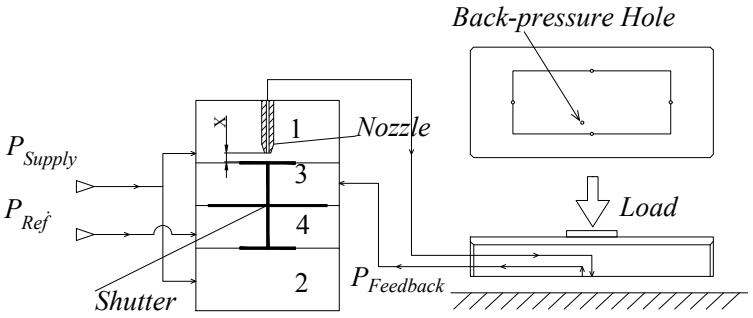

Fig. 4: Functional scheme of the active pad.

3 The lumped parameter model

The proposed actively compensated pad was modelled through a lumped parameter model consisting of pneumatic capacitances and resistances. Figure 5 shows the equivalent pneumatic model of the system. Starting from the upstream, the valve is modelled as a variable resistance R_1 and volume V_1. The variable resistance R_1 is due to the pressure loss occurring at the outlet of the nozzle ($d_n = 1\ mm$) and it can be tuned depending on the initial nozzle-shutter distance x. Consequently, the pressure within the chamber of the valve P_1varies accordingly with x. The restrictors of the pad are modelled as four parallel resistances (R_2). P_2 is the pressure at the outlet of each orifice, whereas the air gap pressure inside the grooved rectangular supply line is considered constant (P_{gap}) which is evaluated through the function L. The expression of this mean pressure is evaluated through the following semi-empirical formula [2,3]:

$$P_{gap} = \left[1 - 0.02^{\left(\frac{5}{h}\right)}\right] (P_2 - P_a) + P_a \tag{1}$$

The pressure P_{gap} is used as a feedback pressure to suitably modify the nozzle-shutter distance x on the basis of the following equation:

$$\begin{cases} x = x_{by-pass}; & x < x_{by-pass} \\ x = x_0 + A_s \dfrac{\left(P_{gap} - P_{Ref}\right)}{k_m}; & x > x_{by-pass} \end{cases} \tag{2}$$

where, A_s is the is the area of the shutter, k_m is the stiffness related to the membranes, x_0 is the initial nozzle-shutter distance and P_{Ref} is the reference pressure of the valve (see section

2). $x_{by-pass} = f(P_{Ref})$ is a threshold distance proportional with P_{Ref} that was inserted to take into account the air leakages experienced when the shutter is very close to the nozzle. The model considers a linear pressure distribution between the central region (P_{gap}) and the edge of the pad (P_a). The air mass flow rates passing through the resistances of the system are modelled through the equation proposed in [23]:

$$G_i = K_T cd_i \frac{0.685}{\sqrt{R\,T}} A_i P_{up} \sqrt{1 - \left(\frac{\frac{P_{down}}{P_{up}} - 0.528}{1 - 0.528} \right)^2} \tag{3}$$

where, K_T is the square root of the ratio between the valve (293 K) and the reference absolute temperatures (273 K). A_i, cd_i, P_{down} and P_{up} are the area, discharge coefficient and the inlet and outlet pressures of the ith lumped resistance ($i = 1, 2$). The discharge coefficients are assumed to be functions of the Reynolds' Number (Re_i) related to the flow of each resistance.

$$cd_i = 1.05(1 - 0.3\, e^{-0.005\, Re_i}) \tag{4}$$

$$Re_1 = \frac{G_1}{\pi\, \mu d_n} \tag{5}$$

where, d_n is the nozzle diameter, μ is the dynamic viscosity and G_1 is the air mass flow rate related to the nozzle. The presence of the shallow groves of the pad was taken into account by considering the following equivalent cross-section and modified Reynolds' Number:

$$A_2 = \pi\, d_s\, h + w_g\, h_g \tag{6}$$

$$Re_2 = \frac{G_2\, h}{\mu A_2} \tag{7}$$

Finally, the load carrying capacity of the pad is computed as follows:

$$F_p = \left[ab + AB + \frac{(Ab + aB)}{2} \right] \frac{(P_{gap} - P_a)}{3} \tag{8}$$

The adopted numerical procedure employs the pseudo-unsteady method [20] which is similar to those employed in [11]. This technique consists in two main consequent and iterative steps:

- Computing the pad performance by imposing the air gap height
- Using the results of the previous step as a starting point for the second part of the code where the air gap height is computed through the equilibrium equation of the pad depending on the value of the external load.

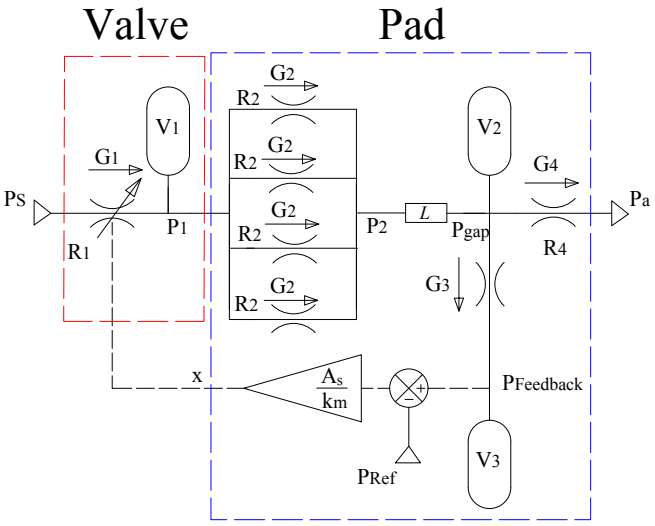

Fig. 5: Pneumatic scheme of the controlled pad.

Figure 6 shows a scheme of the test bench adopted to assess the static performance of the proposed active pad. Static characterizations are performed by applying and external load to the pad and simultaneously measuring the related force, air gap height, air consumption and the feedback pressure within the valve (see section 2). The pad under test is placed on a metallic counterpad which is fixed on a granite base. The external force is applied by acting on a handwheel that, thanks to a lead screw arrangement, produces a translation of a mechanical loading chain composed of a movable link, a load cell and a spherical tip. The air gap variations are indirectly evaluated by measuring the displacement of the upper surface of the pad by means of four capacitive sensors. The air consumption of the pad is measured through a flowmeter located upstream of the pad, whereas the feedback pressure is assessed with the aid of a digital pressure gauge.

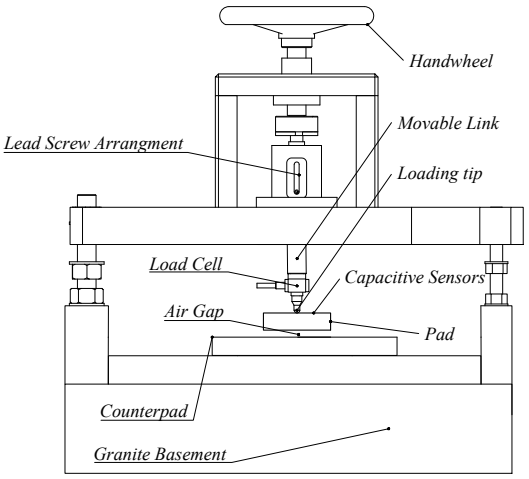

Fig. 6: Test bench.

5 Results and conclusions

To evaluate the effect of varying the initial shutter-nozzle distance x_0, the static tests were performed in the presence of different constant absolute reference pressures: P_{Ref}= 0.1, 0.15, 0.2, 0.25, 0.275 and 0.3 MPa. Figures 7 and 8 compare the experimental and numerical results obtained from the static characterization of the proposed prototype. Figures 7 and 8 show the load carrying capacity and the air consumption curves of the active pad. Numerical and experimental results are in good agreement concerning the load capacity. Conversely, probably because of the pad deformation and the non-planar shape of the surface [24,25], they present a shift as regards air consumption. It is possible to see that some of the curves plotted in these two graphs present distinctive trends which are different from those of the common characteristic curves. In particular, considering the graphs obtained in the presence of a non-zero relative reference pressure ${P_{Ref}}^{Rel}$, three different regions can be distinguished depending on the air gap height. Starting from higher flight heights, a by-pass, a regulation and a saturation region can be identified in order. In the by-pass region, the load applied on the pad is not high enough to generate a feedback pressure (chamber 3, see Figure 4) sufficient to create a clearance between the nozzle and the shutter ($x < x_{by-pass}$). In these instances, the pressurized air supplied to the pad is due to leakages because the closure of the nozzle is not perfect. When the external load increases, the nozzle-shutter distance increases with the feedback pressure ($x>x_{by-pass}$ and $P_{Feedback}>P_{Ref}$). This makes it possible to increase the air gap height by regulating the air supplied to the pad. It should be noted that the curves present some parts which are characterized by negative stiffness. This means that, in these regions, the action of the valve generates an over-compensation. On further increasing the applied load, the nozzle-shutter distance becomes so high that the nozzle saturates (this condition corresponds to the maximum air consumption (see Figure 8).

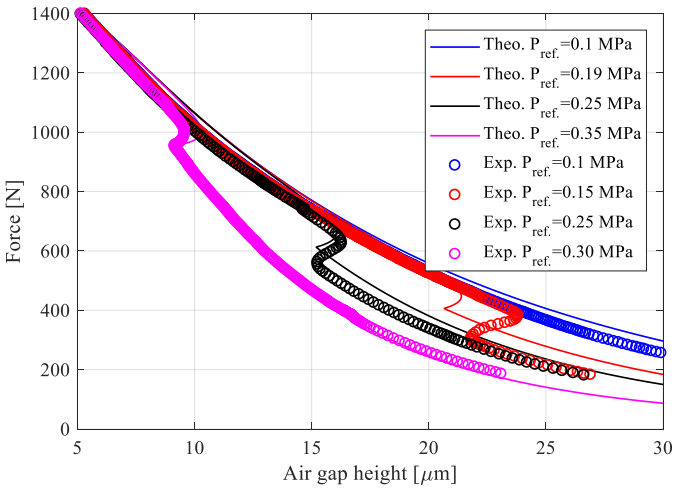

Fig. 7: Experimental and numerical load capacity of the active pad.

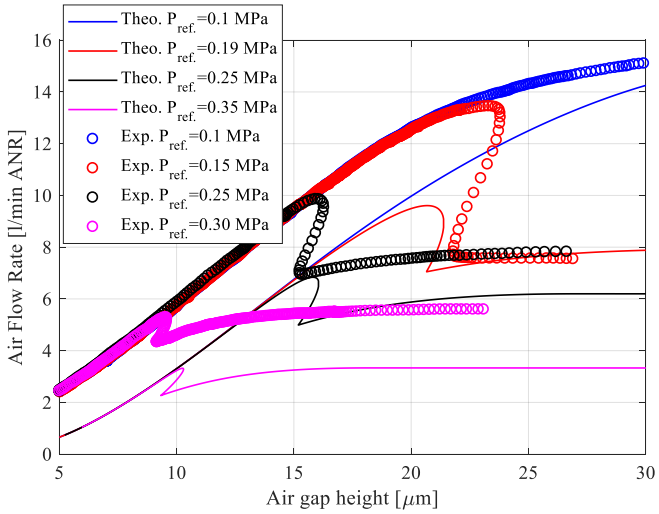

Fig. 8: Experimental and numerical air consumption of the active pad.

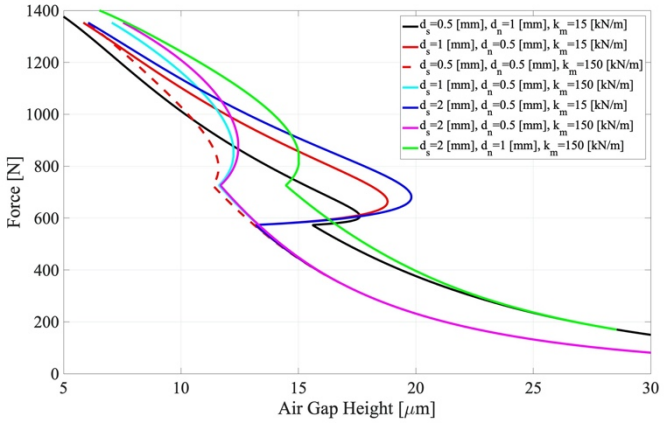

Fig. 9: The effect of varying the stiffness of the membranes and the diameters of the nozzle and the restrictors on the pad load capacity.

When this condition is reached, every additional increase of the applied load cannot modify the air flow supplied to the pad that starts reducing. Moreover, the position of the regulation zone can be shifted by suitably regulating the initial reference pressure P_{Ref} (see Figures 7 and 8). Increasing the reference pressure tends to shift the regulation area towards lower flight heights. After this saturation, the system works as in the presence of a zero relative reference pressure, i.e., like a common air pad. It is interesting to see that each regulation region presents a portion characterized by almost infinite stiffness. In this case, the membrane stiffness identified via the numerical model was 50 kN/m.

In the final phase, the numerical model was used to investigate the effect of varying different parameters on the load capacity of the pad. These simulations were performed by considering different membrane stiffnesses (k_m=15 and 150 kN/m) and different diameters of the nozzle (d_n=0.5 and 1 mm) and the supply restrictors (d_s=0.5, 1 and 2 mm) of the pad

(see Figure 9). It was found that the regulation zone enlarges slightly on increasing the ratio between the nozzle and the restrictor diameters. Moreover, increasing the stiffness of the membranes reduces the overcompensation of the valve leading to regulation zones characterized by almost infinite stiffnesses.

6 Conclusions

This work studied the static performance of new prototype of active aerostatic bearing consisting in the integration of a commercial pad and a custom-built pneumatic regulating valve. The performance of the prototype was investigated through experimental tests and by means of a numerical lumped model. It was shown that the presence of the valve makes it possible to obtain a regulation zone where the static performance of the pad can be improved by obtaining infinite and even negative stiffness (overcompensation). It was found that varying the reference pressure inside the valve makes it possible to modify the position of the regulation zone. The numerical results show that the stiffness of the pad can be significantly increased by a suitable tuning of the membrane stiffness and the diameters of the nozzle and the restrictors. In particular, numerical results suggest a substantial increase of the membrane stiffness (about ten times the current one). Eventually, the proposed method may have the potential to become a good and a cost-effective method to enhance the static performance of aerostatic pads.

References

1. L. Lentini, M. Moradi, and F. Colombo, Tribology in Industry **Vol. 40**, No. 2, pp. 165-182, (2018).
2. F. Colombo, L. Lentini, T. Raparelli, A. Trivella, and V. Viktorov, Mechanisms and Machine Science, **Vol. 68**, pp 490-497, (2019).
3. F. Colombo, L. Lentini, T. Raparelli, A. Trivella, and V. Viktorov, Mechanisms and Machine Science, **Vol. 67**, pp. 678-686, (2019).
4. T. Nakamura and S. Yoshimoto, Tribology International **Vol. 29(2)**, pp 145-152, (1996).
5. S. Yoshimoto, J. Tamura, and T. Nakamura, Tribology International **Vol. 32(12)**, pp 731-738, (1999).
6. F. Colombo, L. Lentini, T. Raparelli, A. Trivella, and V. Viktorov, AIMETA 2017 - Proceedings of the 23rd Conference of the Italian Association of Theoretical and Applied Mechanics, **Vol. 4**, pp. 506-517 (2017).
7. T. Raparelli, V. Viktorov, F. Colombo, and L. Lentini, Precision Engineering **Vol. 44**, pp. 1-12 (2016).
8. S. Yoshimoto, Y. Anno, and Y. Hirakawa, JSME International Journal. Ser. C, Dynamics, Control, Robotics, Design and Manufacturing **Vol. 37(2)**, pp. 369-375, (1994).
9. P. M. Newgard and R. L. Kiang, A S L E Transactions **Vol. 9(3)**, pp. 311-317 (1966).
10. D. Ghodsiyeh, F. Colombo, T. Raparelli, A. Trivella, and V. Viktorov, Tribology International **Vol. 109**, pp 328-335 (2017).
11. D. Ghodsiyeh, F. Colombo, L. Lentini, T. Raparelli, A. Trivella, and V. Viktorov, Tribology International **Vol. 141**, 105964 (2020).

12. M.-F. Chen and Y.-T. Lin, JSME International Journal Series C **Vol. 45(2)**, pp. 492-501 (2002).
13. F. Al-Bender, Precision Engineering **Vol. 33(2)**, pp. 117-126 (2009).
14. G. Aguirre, F. Al-Bender, and H. Van Brussel, Precision Engineering **Vol. 34 (3)**, pp. 507-515 (2010).
15. F. Colombo, L. Lentini, T. Raparelli, and V. Viktorov, Meccanica, **Vol. 52**(15), pp. 3645-3660 (2017).
16. F. Colombo, L. Lentini, T. Raparelli, and V. Viktorov, Mechanisms and Machine Science, **Vol. 47**, pp. 441-448 (2017).
17. S. Morosi and I. F. Santos, Proceedings of the Institution of Mechanical Engineers, Part J: Journal of Engineering Tribology **Vol. 225(7)**, pp. 641-653 (2011).
18. S. Morosi and I. F. Santos, Tribology International **Vol. 44(12)**, pp. 1949-1958 (2011).
19. F. G. Pierart and I. F. Santos, Tribology International **Vol. 96**, pp. 237-246 (2016).
20. R. Peyret and H. Viviand, in Recent Advances in the Aerospace Sciences: In Honor of Luigi Crocco on His Seventy-Fifth Birthday, edited by C. Casci and C. Bruno (Springer US, Boston, MA, 1985), pp. 41–71.
21. T. Raparelli, V. Viktorov, A. Manuello Bertetto, and A. Trivella, in Proceedings of the First 2000 AIMETA International Tribology Conference (2000), pp. 693–700.
22. G. Belforte, T. Raparelli, V. Viktorov, and A. Trivella, in 5th JFPS International Symposium on Fluid Power (S. Yokota, 2002).
23. G. Belforte, T. Raparelli, and V. Viktorov, Journal of Tribology **Vol. 124 (4)**, pp. 716-724. (2002).
24. F. Colombo, L. Lentini, T. Raparelli, V. Viktorov, and A. Trivella, Mechanisms and Machine Science, **Vol. 73**, pp. 3929-3937 (2019).
25. F. Colombo, L. Lentini, T. Raparelli, V. Viktorov, and A. Trivella, Mechanisms and Machine Science, **Vol. 73**, pp. 3919-3928 (2019).